AIAA Journal
Vol. 47, No. 12, December 2009

Hysteretic Phenomenon of Underexpanded Moist Air Jet

Yumiko Otobe,* Tsuyoshi Yasunobu,† and Hideo Kashimura‡
Kitakyushu National College of Technology, Kitakyushu 802-0985, Japan
Shigeru Matsuo§ and Toshiaki Setoguchi§
Saga University, Saga 840-8502, Japan
and
Heuy-Dong Kim¶
Andong National University, Andong 760-749, Republic of Korea

DOI: 10.2514/1.38023

Moist air jets, corresponding to the range of moderately underexpanded to strongly underexpanded conditions, have been investigated with the help of computational fluid dynamics methods. The equations for nucleation rate and droplet growth are incorporated into the unsteady, compressible Navier–Stokes equations. A third-order total variation diminishing finite difference scheme with monotonic upstream schemes for conservation lows is employed to discretize the spatial derivatives of the governing equations. The experiment is performed to validate the computational predictions. The initial degree of supersaturation is changed to obtain different values of the relative humidity of moist air. The pressure ratio is changed to investigate the characteristic behavior of the jets generated during the transient processes of startup and shutdown. The results obtained show that underexpanded air jet produced during the startup transient of jet behaves different from the shutdown transient process, leading to a hysteretic phenomenon of underexpanded jet. It is also known that the moist air jet reduces the hysteretic phenomenon compared with the dry air jet, and that nonequilibrium condensation that occurs in the underexpanded moist air jet is responsible for these findings.

Nomenclature

c_p	=	specific heat at constant pressure
D_e	=	nozzle exit diameter
D_m	=	Mach disk diameter
MR	=	Mach reflection
p	=	static pressure
RR	=	regular reflection
S_0	=	initial degree of supersaturation
x, r	=	cylindrical coordinates of jet
x_t	=	distance from nozzle exit to Mach disk
φ	=	ratio of nozzle supply pressure to back pressure
ξ	=	calculation time

I. Introduction

UNDEREXPANDED freejet is one of the simplest flows that has a number of practical applications ranging from the design of rocket propulsion systems to industrial areas using high-pressure gas. A great deal of works have been made to investigate the major features of sonic freejets [1–3]. According to these studies, the flow pattern of a jet issuing from a nozzle or an orifice depends primarily on the ratio of the pressure at the nozzle exit to the ambient pressure. Depending on this pressure ratio, three types of jets are possible: subsonic, moderately underexpanded, and highly underexpanded jets. The values of pressure ratio separating these three flow patterns are dependent on the specific heat of the gas, although the variation from one gas to another gas is quite small [4,5].

In cases of subsonic jets, the pressure at the exit of the nozzle is always matched with the ambient pressure, and the jet propagation direction at the nozzle exit is parallel to the nozzle wall. However, when the jet becomes underexpanded the pressure at the exit of nozzle is higher than the ambient pressure. With an increase in the pressure ratio, the jet is changed from the moderately underexpanded to the strongly underexpanded jets. These two jets are mostly distinguished by the appearance of the Mach disk inside the jet [6–8].

Many previous studies have shown that the Mach disk is one of the most important factors specifying the highly underexpanded sonic jets. Billig et al. [9], Saito et al. [10] and Narayanan and Damodaran [11] have investigated the diameter of Mach disk, the distance from the exit of nozzle to the Mach disk, and the configuration of the jet boundary. They have documented that all these quantities are a function of the pressure ratio only. Addy [12] has shown with some experimental work using several different nozzles that the nozzle configuration does not affect the distance of Mach disk. However, he has pointed out that it can somewhat influence the diameter of Mach disk. Many other researchers [13,14] have reported results similar to the work of Addy [12].

Cumber et al. [14] have collected the experimental data obtained by many other researchers and showed that the distance of Mach disk correlates quite well with the pressure ratio, but the correlation in the diameters of Mach disk is relatively poor. They did not give detailed explanation for this poor correlation, and vaguely inferred that it could result from the difference of the nozzle geometries used in each experiment. Recently, Matsuo et al. [15] and Otobe et al. [16] have reported that the poor correlation in the Mach disk diameters is due to the vena contracta phenomenon formed in the orifice nozzles used in various experimental work, and they have demonstrated a good correlation using an imaginary nozzle throat concept based on the vena contracta.

Several researchers have investigated the effects of the working gas on supersonic freejets [17,18]. According to these results, the specific heat ratio of the working gas influences the jet pressure ratio as well as the convective velocities of the gas particles. Recently, the supersonic jets have been often applied in power plants and industrial manufacturing processes. In these applications, the working gas is usually steam or moist air, which has not received the same level of

Received 11 April 2008; revision received 2 September 2009; accepted for publication 3 September 2009.

*Research Associate, Department of Control and Information Systems Engineering, 5-20, Shii Kokuraminami.
†Associate Professor, Department of Control and Information Systems Engineering, 5-20, Shii Kokuraminami.
‡Professor, Department of Control and Information Systems Engineering, 5-20, Shii Kokuraminami.
§Professor, Department of Mechanical Engineering, 1, Honjo.
¶Professor, School of Mechanical Engineering, 388, Songchon. Senior Member AIAA (Corresponding Author).

attention in supersonic jet technologies as single-phase gases. Baek et al. [19] and Otobe et al. [20] have experimentally and numerically investigated the Mach disk that is formed in underexpanded moist air jet. They have reported that the moist air jets are qualitatively similar to the dry air jets, but nonequilibrium condensation in the moist air jet affects the Mach disk diameter because the nonequilibrium condensation of moisture component changes the local flow states just upstream of the Mach disk.

As previously mentioned, if the pressure ratio and nozzle geometry are given, the structures of underexpanded jet are well known. As the pressure ratio increases over a certain critical value corresponding to a sonic condition at the exit of nozzle, regular reflection of shock wave occurs in the weakly underexpanded jet. Then, as the pressure increases further, the regular reflection transitions to Mach reflection leading to the Mach disk on the jet axis. On the contrary, the Mach reflection reduces again to the regular reflection, as the jet pressure ratio decreases.

Recently, Irie et al. [21] have observed that a hysteresis phenomenon of the underexpanded dry air jet is produced during the transient processes of jet pressure ratio, in which the jet flow obtained in the startup transient is different from that in the shutdown transient. In many industrial and engineering applications of underexpanded jets, the jet pressure ratio is found to change during a process. However, to date only a few research works have been devoted to the jet hysteresis. The physical reasoning as to what causes this phenomenon is still not satisfactorily known. No research has been done to investigate the hysteresis phenomenon in underexpanded moist air jets thus far.

In the present study, underexpanded moist air jets from moderately underexpanded to strongly underexpanded conditions have been investigated with the help of a computational fluid dynamics method. The jet pressure ratio is varied to obtain the hysteresis phenomena. Quasisteady computational analysis is carried out to numerically solve the axisymmetric/compressible Navier–Stokes equations. Initial relative humidity at the nozzle supply is assumed to get different moist air jets. The present computations are validated with the experimental data. The results obtained show that the hysteresis behavior appears in both dry and moist air jets, but the moist air jets lead to much less hysteresis compared with the dry air jets.

II. Computational Analysis

A. Governing Equations

Assumptions employed in the present computation of the two-phase supersonic jet flow are as follows: both velocity slip and temperature difference between condensate particles and gas mixture do not exist, and the effect of the condensate particles on pressure is neglected. The governing equations are the unsteady compressible Navier–Stokes equations and droplet growth equation [22] written in an axisymmetric coordinate system (x, r) (r represents radial distance from centerline)

$$\frac{\partial U}{\partial t} + \frac{\partial E}{\partial x} + \frac{\partial F}{\partial r} = \frac{\partial R}{\partial x} + \frac{\partial S}{\partial r} + \frac{1}{r} H_1 + H_2 + Q \tag{1}$$

where U is the vector of conservative variables, E and F are inviscid flux vectors, and R and S are viscous flux vectors. H_1, H_2, and Q are the source terms of axisymmetry, turbulence, and condensation, respectively. The rate equation of condensate mass fraction generated by homogeneous nucleation is written as

$$\frac{\mathrm{d}g}{\mathrm{d}t} = \frac{4\pi}{3} \cdot \rho_l \cdot r_c(t)^3 \cdot \frac{I(t)}{\rho_{mi}(t)} + \int_{-\infty}^{t} 4\pi \cdot \rho_l \cdot \frac{I(\tau)}{\rho_{mi}(\tau)} \cdot \frac{\partial r_l(t,\tau)}{\partial t} \cdot r_l(t,\tau)^2 \,\mathrm{d}\tau \tag{2}$$

In Eq. (2), g and t are the condensate mass fraction and the time, respectively; ρ is the density, and r_c and I are critical droplet radius and nucleation rate per unit time and unit volume, respectively. Subscripts mi and l refer to mixture and liquid, respectively. I, r_c, $\mathrm{d}r/\mathrm{d}t$, ρ_l, surface tension, saturation vapor pressure of condensate droplet with a radius of r, latent heat, and coefficients are given in detail in [22–24]. The latent heat is given by a function of temperature

$$L(T) = L_0 + L_1 T \ \mathrm{J/kg} \tag{3}$$

where the coefficients are given by

$$L_0 = 3105913.39 \ \mathrm{J/kg}, \qquad L_1 = -2212.97 \ \mathrm{J/kg/K}$$

Validation of the condensation model using these equations and quantities can be found in [22–24].

To close the governing equations, the modified k-R model [25,26] is employed in computations. The turbulent kinetic energy and the undamped eddy viscosity are determined by the following transport equations:

$$\frac{\partial(\rho_{mi}k)}{\partial t} + \frac{\partial(\rho_{mi}ku)}{\partial x} + \frac{\partial(\rho_{mi}kv)}{\partial r} = \frac{\partial}{\partial x}\left[\left(\mu_l + \frac{\mu_t}{\sigma_k}\right)\cdot\frac{\partial k}{\partial x}\right] + \frac{\partial}{\partial r}\left[\left(\mu_l + \frac{\mu_t}{\sigma_k}\right)\cdot\frac{\partial k}{\partial r}\right] + P_k - \frac{(\rho_{mi}k)^2}{\rho_{mi}R} \tag{4}$$

$$\frac{\partial(\rho_{mi}R)}{\partial t} + \frac{\partial(\rho_{mi}Ru)}{\partial x} + \frac{\partial(\rho_{mi}Rv)}{\partial r} = \frac{\partial}{\partial x}\left[\left(\mu_l + \frac{\mu_t}{\sigma_R}\right)\cdot\frac{\partial R}{\partial x}\right] + \frac{\partial}{\partial r}\left[\left(\mu_l + \frac{\mu_t}{\sigma_R}\right)\cdot\frac{\partial R}{\partial r}\right] - \frac{\rho_{mi}C_\mu}{\sigma_R}\cdot\left[\left(\frac{\partial R}{\partial x}\right)^2 + \left(\frac{\partial R}{\partial r}\right)^2\right] + (2 - C_{R1})\cdot\frac{R}{k}\cdot P_k - (2 - C_{R2})\cdot\rho_{mi}k \tag{5}$$

where P_k is the turbulent production modeled in term of the Boussinesq concept

$$P_k = \left[\mu_t\left(\frac{\partial u_i}{\partial x_j} + \frac{\partial u_j}{\partial x_i} - \frac{2}{3}\cdot\frac{\partial u_k}{\partial x_k}\cdot\delta_{ij}\right) - \frac{2}{3}\rho_{mi}k\delta_{ij}\right]\frac{\partial u_i}{\partial x_j} \tag{6}$$

The undamped eddy viscosity R [27] is given by

$$R \equiv \frac{k^2}{\varepsilon} \tag{7}$$

where k is the turbulent kinetic energy and ε is its dissipation. In Eqs. (5) and (6), u_i and u_j are the Cartesian mean velocity components, x_i and x_j are the corresponding coordinates, and μ_l and μ_t are the molecular and eddy viscosities, respectively.

In the present computations, a limiter function [28] is introduced to suppress the instability in the region of Mach disk as

$$P_k = \min[P_k, C_2 \cdot C_b \cdot \rho_{mi} \cdot \varepsilon \cdot Re/C_1] \tag{8}$$

where C_b is a limiting parameter determined by empirical approach, and

$$C_1 = 1.44, \qquad C_2 = 1.92 \times [1 - 0.3\exp(-R_T^2)], \qquad C_b = 1.001$$
$$C_\mu = 0.09, \qquad \sigma_k = 1.0, \qquad \sigma_R = 1.080, \qquad C_{R1} = 1.44$$
$$C_{R2} = 1.92$$

The eddy viscosity is given by

$$\mu_t = C_\mu \cdot f_\mu \cdot \rho_{mi} \cdot R \tag{9}$$

where the near-wall damping function f_μ is given as

$$f_\mu = \frac{\tanh(\alpha \cdot R_T)}{\tanh(\beta \cdot R_T)} \tag{10}$$

where

$$R_T = \frac{\rho_{mi}k^2}{\mu_l \varepsilon} = \frac{\rho_{mi}R}{\mu_l}, \qquad \alpha = 0.005, \qquad \beta = \frac{C_\mu^{\frac{3}{4}}}{\kappa_k} \tag{11}$$

The governing equation systems that are nondimensionalized with reference values at the inlet conditions upstream of the nozzle are mapped from the physical plane into a computational plane of a general transformation. A third-order TVD (total variation diminishing) finite difference scheme with monotonic upstream schemes for conservation lows [29] is used to discretize the spatial derivatives of the governing equations, a second-order-central difference scheme is used for the viscous term, and a second-order fractional step for time integration.

B. Boundary Conditions

A cylindrical straight nozzle has a diameter of $D_e = 12.7$ mm (see Fig. 1). The nozzle is composed of a convergent curved entrance wall that has a radius of curvature $R = D_e$, and the following straight wall having a length of $0.4D_e$. This is exactly the same as that used by Addy [12], so that the present computational results can be validated with his data as well as the present experiments.

Moist air is assumed as the working gas, and its initial relative humidity at the nozzle supply is given by a function of the initial degree of supersaturation S_0. The jet pressure ratio of moist air is defined as φ, the ratio of total pressure p_0 at the nozzle supply to back pressure p_b. In the present study, φ varies from 3.0 to 6.2, and the initial degree of supersaturation S_0 of moist air is varied between 0 (dry air) and 0.8. The upstream total temperature T_0 and total pressure p_0 are assumed to be maintained constant at 298.15 K and 101.3 kPa, respectively, through the whole computation.

The fixed upstream boundary conditions were applied to the upstream boundary of the computational domain, and the downstream boundary was subject to the outflow conditions. Adiabatic and no-slip boundary conditions were applied to the solid wall surfaces. Further, condensate mass fraction was assumed to be zero at the nozzle wall surfaces. According to several preliminary computations, it was known that numerical waves were propagating far upstream of the nozzle inlet. Hence, the upstream domain in the present computations extends to the distance of $80De$ upstream from the nozzle exit, whereas the downstream domain covers the region of $150De$ and $50De$ from the nozzle exit, in the x and r directions, respectively. This wide computational domain was required to ensure the computational domain independent solutions.

Figure 1 shows a typical grid system employed in the present computations. The computational grids were clustered in the flow regions with large gradient such as the wall boundary layer, shock wave, and nozzle exit. The computational grids closest to the nozzle walls are located 0.00154 mm away from the walls. Several computations were performed on different computational meshes to investigate the grid-independent solutions. The peak pressure and location of shock wave in the jets were checked on different grid meshes (117×31, 165×43, 235×62, 353×93, and 470×124). The solutions seemed to change with the smaller grids employed, but for the grids over 0.1 million points they did not change appreciably (the present computations were performed on the 235×62 mesh).

C. Computational Procedure

The hysteresis cycle has been often reported in several flowfields due to the nonlinear nature inherent in the flow under consideration. Such flows can be computed by numerical simulations [30], in which the flow boundary conditions are systematically changed to obtain each of the quasisteady solutions. Detailed procedure can be found in [30]. Figure 2 shows the computational procedure for the process of the shutdown transient, in which the pressure ratio is decreased. The steady underexpanded jet of $\varphi = \varphi_{st}$ is computed and the resulting solutions are used as the initial conditions for the first step of the process of the shutdown transient. In the second step, the pressure ratio is decreased by $\Delta\varphi$ and the computation is repeated until the transient process is completed, thus leading to a quasisteady state as indicated by the black circle. The computed quasisteady solutions are used again as the initial conditions for the next step [30]. Consequently the final quasisteady solutions are obtained for the pressure ratio of φ_{fi}. On the contrary, for the process of the startup transient, in which the pressure ratio is increased, the final quasisteady solutions are used again as the initial conditions. For reference, in the present study $\varphi_{st} = 6.2$, $\varphi_{fi} = 3.0$, $\Delta\varphi = 0.1$, and $\xi = 20000$. Through such a series of computations, the quasisteady solutions obtained during both the startup and shutdown transients are compared to investigate the hysteretic behaviors of the underexpanded moist air jets.

III. Experimental Work

Experimental work has been conducted to validate the present computations. Figure 3 shows the experimental apparatus. A simple jet facility has been fabricated to easily visualize the hysteretic behavior of the jet. A plenum chamber is placed upstream of the convergent nozzle. Room air at atmospheric conditions enters the plenum chamber, and a moisture generator and heater control the

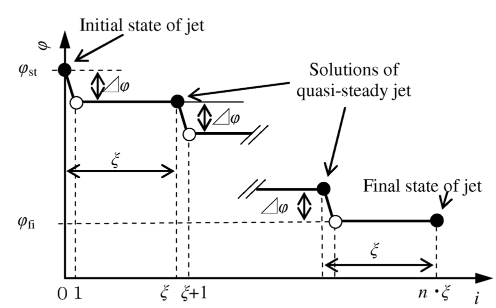

Fig. 2 Computation procedure to simulate the processes of shutdown and startup transients.

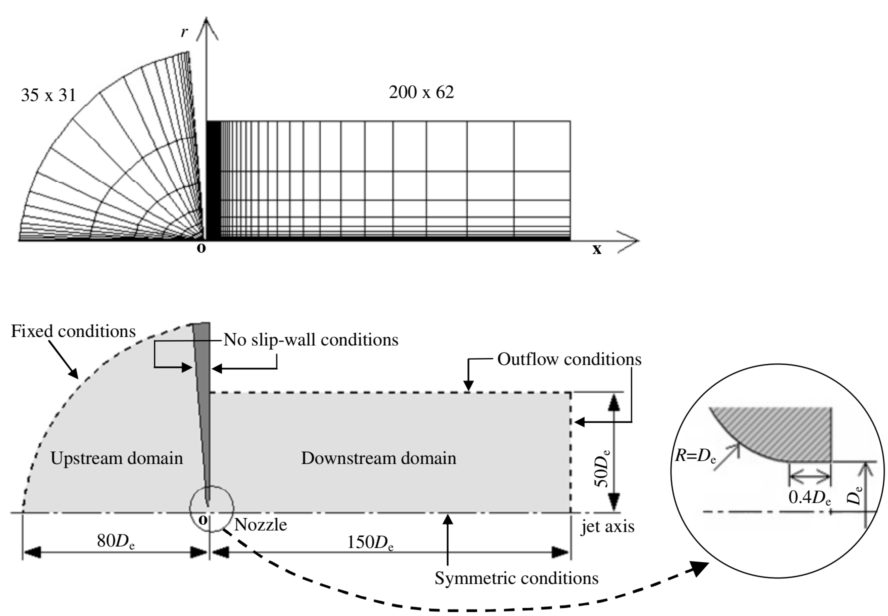

Fig. 1 Computational grid mesh and boundary conditions.

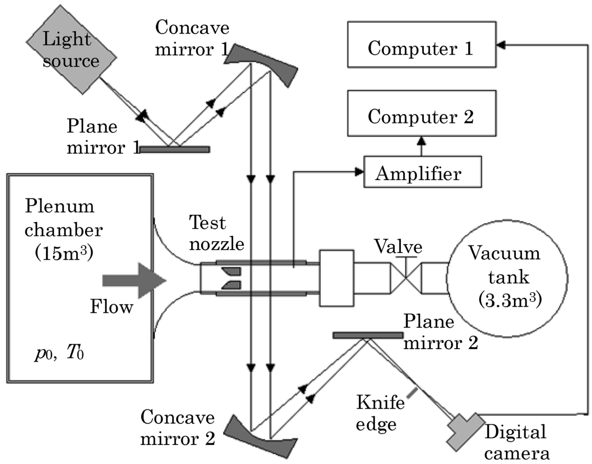

Fig. 3 Schematic view of experimental facility.

flow conditions inside it. The test section is placed downstream of the nozzle and the optical glass windows are installed on both the side walls of the test section for flow visualization. The test section is connected to a large vacuum chamber via a ball valve system. The moist air, which flows through the convergent nozzle into the test section, is sucked into the vacuum chamber. The pressures are measured using transducers in the plenum and vacuum chambers. In the experiment, the range of the pressure ratio φ is varied between 3.6 and 6.4. The initial degree of supersaturation S_0 is varied from 0.15 to 0.7. Many visualization pictures have been taken to check on the repeatability in the shock wave locations for both steady and transient jets. The results have shown that they do not significantly change when the experiment is repeated.

IV. Results and Discussion

A. Validation of Steady Jets

The atmospheric air as the working gas contains more or less moisture, depending on the daily weather conditions. In the present experiment, the condition of $S_0 = 0$ that corresponds to the dry air is never achieved due to limited capacity of the dehumidification system employed. The lowest value of S_0 to be reached in the experiment is at most 0.15. Thus, the condition of $S_0 = 0.15$ is assumed to correspond to that of the dry air in present computations.

Figures 4 and 5 show comparisons of the computed and experimental jets for different pressure ratios and S_0. The upper half are the computed isodensity contours and the lower half shows the schlieren pictures. For the dry air of $S_0 = 0$, the jet is slightly underexpanded (see Fig. 4a), and the resulting weak shock waves have the regular reflection at the point P. However, at $S_0 = 0.7$ the shock system becomes the Mach reflection (see Fig. 4b). This difference in the two jets for the same pressure ratio is associated with the latent heat release due to the nonequilibrium condensation of the moisture component. In the case of $\varphi = 6.2$ in Fig. 5a, the dry air jet is strongly underexpanded at the nozzle exit compared with Fig. 4a and thus, leads to the Mach disk on the jet axis. It is again found that the nonequilibrium condensation appreciably influences the shock structure of the dry air jet, as observed in Fig. 5b. It is likely that the diameter of the Mach disk grows with S_0. Unfortunately, the schlieren pictures presented in the lower half are not clear due to three-dimensionality of the flow or, in part, due to the flow unsteadiness; jet boundary, barrel shock, and shear layer are not clearly visible. Nevertheless, it is known from the comparison of the computed and experimental results that the present computations predict the underexpanded dry and moist jets with good accuracy.

Figure 6 shows three typical flow patterns of the underexpanded dry air jets ($S_0 = 0$), which are obtained depending on the pressure ratio. At $\varphi = 3.0$, the jet structure is composed of a multiple of cells and the static pressure distribution along the jet axis is quite similar to a sinusoidal wave (see Fig. 6a). At $\varphi = 4.0$, the barrel shock waves are formed, each of them intersecting on the jet axis. The resulting shock pattern is regular reflection (RR, see Fig. 6b). In this case, the static pressure has a local peak value at the intersection point, which is located at x_t. At $\varphi = 6.0$, the Mach disk occurs at a position of x_t from the nozzle exit, leading to a sudden pressure jump. It is interesting to note that a plateau in the pressure distribution occurs just downstream of the Mach disk, unlike the two cases of $\varphi = 3.0$ and 4.0. The flow is subsonic just downstream of the Mach disk, and the resulting shock pattern poses the Mach reflection (MR). Thus, it

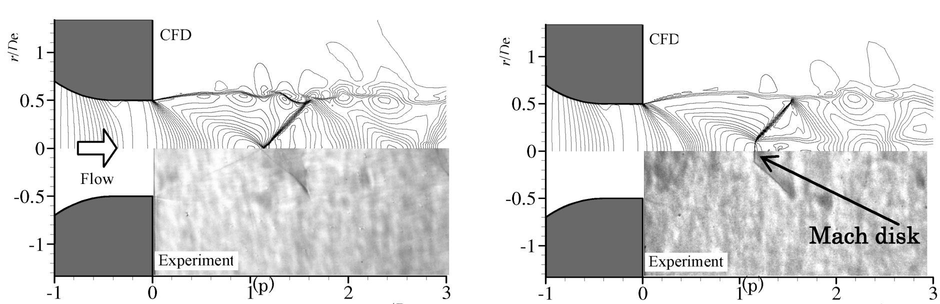

a) S_0=0 b) S_0=0.7

Fig. 4 Comparison between computed and experimental results ($\varphi = 3.8$).

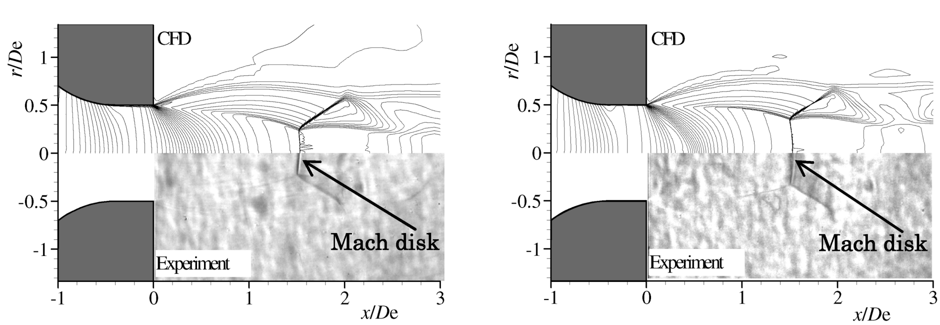

a) S_0=0 b) S_0=0.7

Fig. 5 Comparison between computed and experimental results ($\varphi = 6.2$).

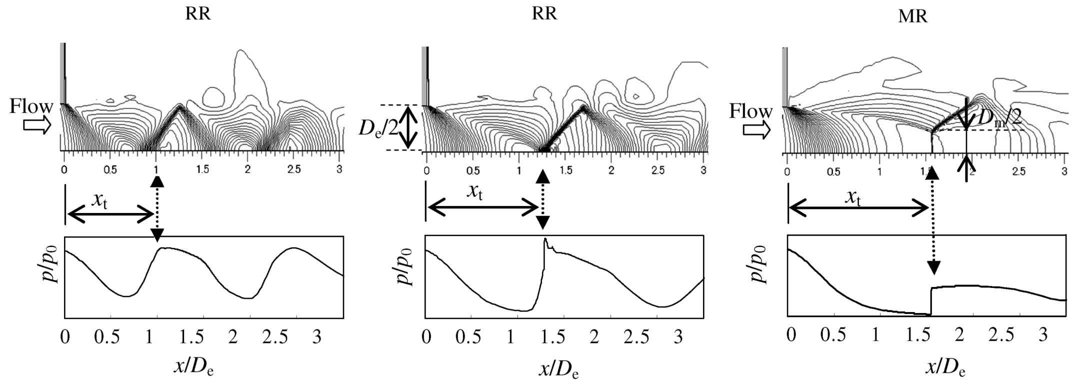

a) φ=3.0 b) φ=4.0 (c) φ=6.0

Fig. 6 Three flow patterns of underexpanded dry air jet ($S_0 = 0$).

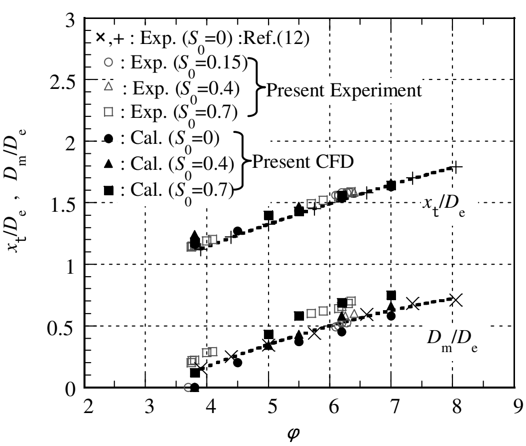

Fig. 7 The variations of x_t/D_e and D_m/D_e with φ.

is clear that the underexpanded dry air jet systematically changes from RR to MR (Figs. 6a–6c) during the startup transient of jet.

Figure 7 represents the validation of the present computations for the steady jets. The prediction results of the present computations for the underexpanded dry and moist air jets are compared with the present experimental data and Addy's data [12]. All of the predicted x_t/De data show that they can be represented by an increasing function of the pressure ratio and are well correlated with the present experimental data, as well as Addy's data. It is likely that S_0 does not significantly influence x_t/De. Meanwhile, the present computations predict the Mach disk diameter (D_m/D_e) well. However, it seems that the diameter of the Mach disk increases with S_0 for a given pressure ratio, as reported in [19]. It is clear that the present computations predict the Mach disk characteristics for both the underexpanded dry and moist air jets with good accuracy.

B. Hysteretic Behavior of Underexpanded Jets

Many researchers have observed the hysteretic behavior occurring during both the startup and shutdown transients in a variety of flowfields. However, detailed reasoning and mechanisms of the hysteresis phenomenon are not yet answered satisfactorily. Recently, Irie et al. [21] have shown that the underexpanded dry air jets behave hysteretically during both the processes of the startup and shutdown transients of the jet. To investigate such a hysteresis phenomenon, the unsteady computational analysis has been performed for both the underexpanded dry and moist air jets, as previously described.

Figure 8 shows the computed isodensity contours for the underexpanded dry (see Fig. 8a) and moist air (see Fig. 8b) jets. For the dry air jets, the jet is strongly underexpanded at $\varphi = 6.2$, and the barrel shock waves reflect from the jet axis, leading to the Mach disk at the location of $x_t/De = 1.57$. A triple point is formed at the intersection point among the three shocks of barrel shock, Mach disk, and reflected shock, and downstream of it the slip stream is generated

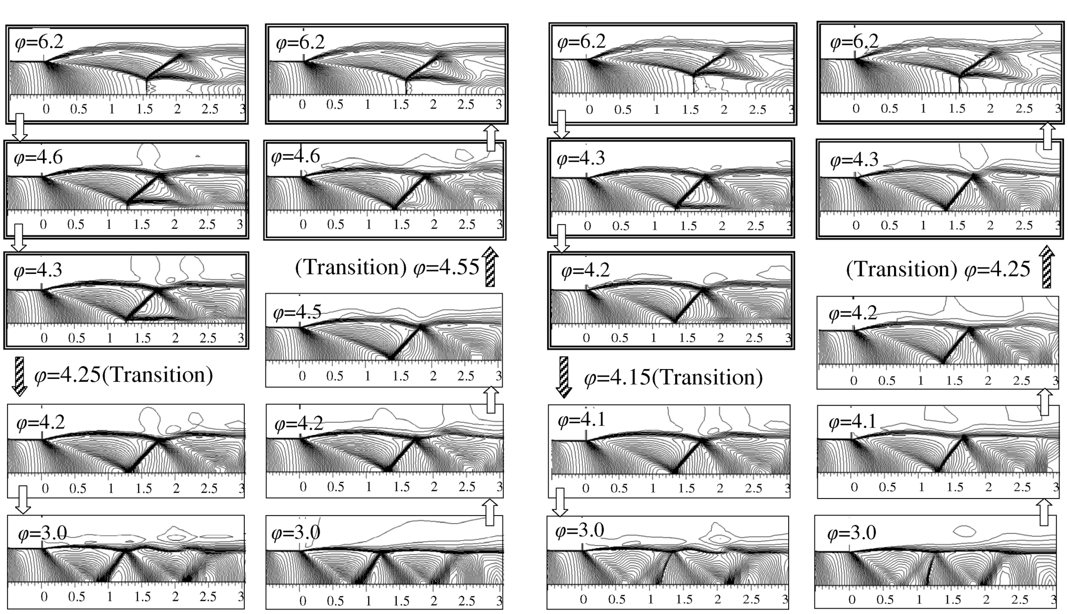

a) S_0=0 b) S_0=0.3

Fig. 8 The underexpanded dry and moist air jets during shutdown and startup transients.

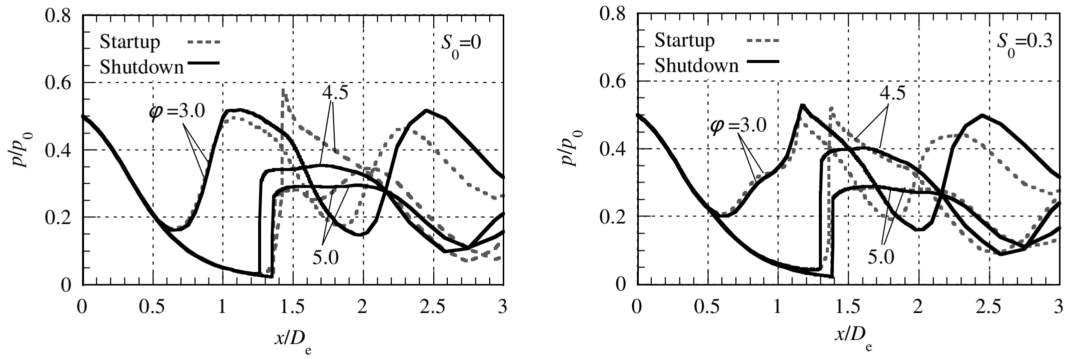

a) S_0=0

b) S_0=0.3

Fig. 9 The static pressure distributions during shutdown and startup transients.

due to the velocity difference in the flows passing over the two oblique shocks and the Mach disk. As φ decreases to 4.6, the Mach disk moves upstream with reduced diameter. At $\varphi = 4.2$, the Mach disk is no longer found and the resulting shock pattern becomes the regular reflection. With further decrease in the pressure ratio, the shock system of the regular reflection moves upstream and its magnitude seems to be weaker. During this shutdown transient of jet, the transition from the Mach disk to the regular reflection flows appears at $\varphi = 4.2$.

Meanwhile, the jet pressure ratio is increased again from the final steady jet state ($\varphi = 3.0$), which has been employed in the previously discussed shutdown transient. As φ increases to 4.2, the regular reflection shocks move downstream with stronger magnitude. The transition from the regular reflection to the Mach reflection flows occurs at $\varphi = 4.55$. With further increase in the pressure ratio, the Mach disk grows and its location moves downstream. At $\varphi = 6.2$, which corresponds to the final steady jet state in the startup transient, the computed flowfield is nearly the same as that employed in the initial conditions in the shutdown transient. From a series of computations, it is found that the pressure ratio at which the transition occurs is significantly different in both the processes of the shutdown and startup transients. Similar hysteretic behavior is also found in the underexpanded moist air jets, as shown in Fig. 8b, where the transition pressure ratio occurs at $\varphi = 4.15$ in the shutdown transient, but at 4.25 in the startup transient. It is, however, noted that the hysteresis phenomenon appears to be reduced in the moist air jet compared with the dry air jet.

Figure 9 shows the computed static pressure distributions along the jet axis for both the underexpanded dry and moist air jets. The solid lines refer to the static pressure distributions obtained in the process of the shutdown transient, and the dotted lines correspond to the process of the startup transient. For the dry air jets, as shown in the shutdown transient, the static pressure of $\varphi = 5.0$ jet suddenly jumps at the location of $x/De = 1.37$, due to the Mach disk. Downstream of it, a plateau occurs in the static pressure distribution. As φ increases to 4.5 the location of the pressure jump moves upstream. With further increase in φ, the steep increase in the static pressure is no longer produced, and the shock system transitions from the Mach reflection to the regular reflection flows. On the contrary, in the process of the startup transient, the static pressure distributions are different mainly near $\varphi = 4.5$, which corresponds to the transition pressure ratio. The pressure jump is much higher compared with that in the process of the shutdown transient, and the plateau static pressures are no longer produced downstream of the Mach disk.

Similar trend is also found in the underexpanded moist air jet ($S_0 = 0.3$) as shown in Fig. 9b. In this case, it is likely that the difference in the pressure distributions obtained in both the processes of the shutdown and startup transients is reduced compared with the dry jet case. It is, thus, believed that the underexpanded moist air jet has less hysteresis. This implies that the nonequilibrium condensation plays a role in reducing the unsteady hysteretic behavior of the underexpanded dry air jets.

More quantitative data for the hysteresis phenomena are presented in Fig. 10, where the locations of the shock reflection during both the

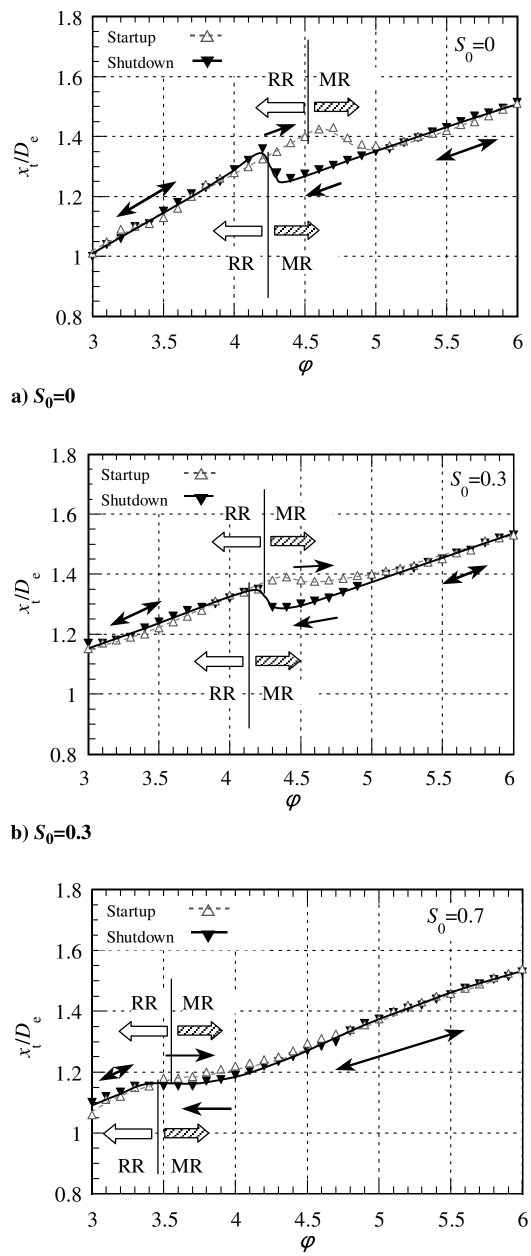

a) S_0=0

b) S_0=0.3

c) S_0=0.7

Fig. 10 Hysteretic behavior in the Mach disk locations during shutdown and startup transients.

processes in the shutdown and startup transients are plotted against the jet pressure ratio. For the dry air jet (see Fig. 10a) in the process of the startup transient, the shock reflection point moves downstream with an increase in φ, and it has a peak at $\varphi = 4.55$, which corresponds to the transition pressure ratio. As φ increases over the transition pressure ratio, the shock reflection point moves a little upstream, and then it moves downstream again with further increase in φ. On the contrary, in the process of the shutdown transient the shock reflection point moves upstream with a decrease in φ, and it has a peak at $\varphi = 4.25$ corresponding to the transition pressure ratio. Then it moves upstream again after moving a little downstream with further decrease in φ. Hysteresis loop in the shock reflection point is found in both the transient processes. It seems that the hysteresis loop is reduced in the moist air jets (see Figs. 10b and 10c).

Figure 11 shows the hysteretic behavior in the diameter of the Mach disk. For the dry air jets, it is found that in the process of the startup transient, the incipient Mach disk occurs at $\varphi = 4.5$ and its diameter increases with an increase in φ. On the contrary, in the process of the shutdown transient it decreases with φ. At $\varphi = 4.25$, the Mach reflection flow transitions to the regular reflection, leading to $D_m/D_e = 0.0$. Therefore, the hysteretic behavior is produced during both the processes of the shutdown and startup transients. It seems that such a hysteresis phenomenon in the diameter of the Mach disk is reduced in the moist air jets (see Figs. 11b and 11c). It is interesting to note that the pressure ratio for the incipient Mach disk decreases with S_0. This is due to the nonequilibrium condensation that occurs depending on a local supersaturation of the flow. Inside the jets, the condensation of the moisture component causes the deceleration of local flow due to the latent heat release. This modifies the local structure of jet, leading to the incipient Mach disk at lower pressure ratio compared with the dry air jets.

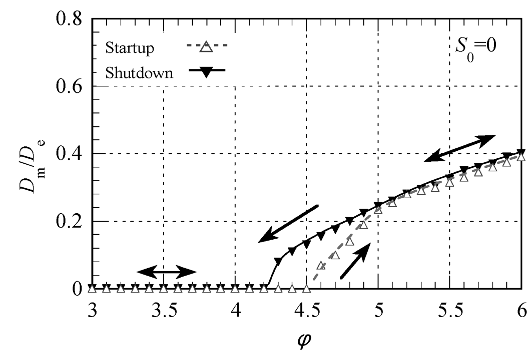

a) S_0=0

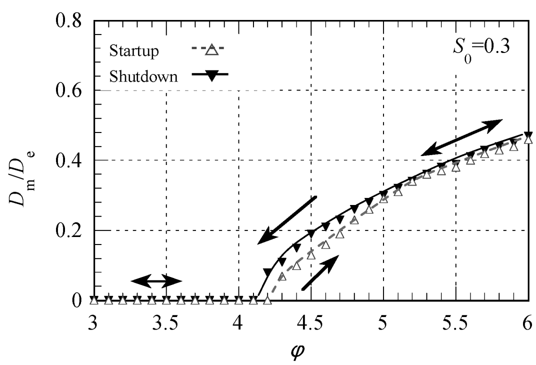

b) S_0=0.3

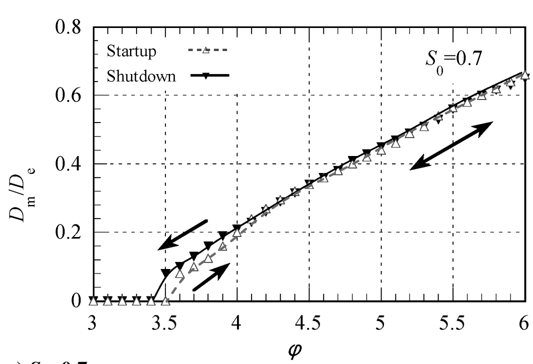

c) S_0=0.7

Fig. 11 Hysteretic behavior in the Mach disk diameters during shutdown and startup transients.

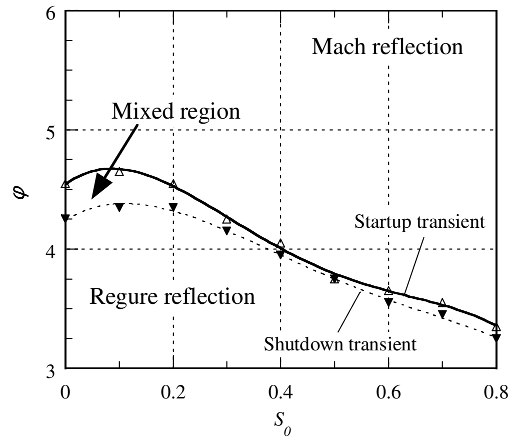

Fig. 12 The limit pressure ratios for the Mach disk flows.

Figure 12 shows the boundary of the limit pressure ratios for the Mach disk flows in both the processes in the shutdown and startup transients. It is found that the limit pressure ratio for the Mach disk flow increases a little with S_0 in the range less than 0.1, but it decreases in the range of S_0 greater than 0.1, regardless of the transient process applied. For example, at $S_0 = 0.2$ it is about 4.5 in the startup transient, and at $S_0 = 0.6$ it reduces to about 3.6. The hysteretic behavior is also found in the limit pressure ratios for the Mach disk flows. It becomes more evident in small S_0 range, but is less so in large S_0 range. This means that the nonequilibrium condensation occurring in the moist air jets alleviates the hysteresis phenomenon of jet.

V. Conclusions

The present study deals with the computational and experimental works to investigate underexpanded dry and moist air jets. The two-dimensional, unsteady, compressible Navier–Stokes equations have been used to numerically solve the flowfield concerning with the hysteretic behavior in both the processes of the shutdown and startup transients of jet. A nucleation rate equation and a droplet growth equation are combined with the governing equation system to simulate nonequlibrium condensation of the moisture component in the underexpanded moist air jets. The present computations accurately predict the major features of the dry and moist air jets as well as the hysteretic behaviors occurring in the shutdown and startup transients of jet. The results obtained show that hysteretic phenomenon is produced both in the underexpanded dry air and moist air jets. Such hysteresis effects are given in terms of the locations and diameters in Mach disk, and they are observed to be reduced with the initial degree of supersaturation of moist air at nozzle supply. This means that the underexpanded moist air jet leads to less hysteresis of jet compared with the dry air jets. It is clear that nonequilibrium condensation which occurs in the underexpanded moist air jet is responsible for these findings.

References

[1] Chuech, S. G., Lai, M. C., and Faeth, G. M., "Structure of Turbulent Sonic Underexpanded Free Jets," *AIAA Journal*, Vol. 27, No. 5, 1989, pp. 549–559.
doi:10.2514/3.10145
[2] Meier, S. G. E. A., Selerowicz, W. C., and Szumowski, A. P., "A Nozzle Generating Low Jet Noise," *Journal of Sound and Vibration*, Vol. 136,

No. 1, 1990, pp. 65–73.
doi:10.1016/0022-460X(90)90938-V

[3] Birkby, P., and Page, G. J., "Numerical Predictions of Turbulent Underexpanded Sonic Jets Using a Pressure-Based Methodology," *Journal of Aerospace Engineering*, Vol. 215, No. 3, 2001, pp. 165–173.
doi:10.1243/0954410011533158

[4] Driftmyer, R. T., "A Correlation of Freejet Data," *AIAA Journal*, Vol. 10, No. 8, 1972, pp. 1093–1095.
doi:10.2514/3.50306

[5] Palmer, J. L., and Hanson, R. K., "Application of Method of Characteristics to Underexpanded, Freejet Flows with Vibrational Noneqilibrium," *AIAA Journal*, Vol. 36, No. 2, 1998, pp. 193–200.
doi:10.2514/2.7501

[6] Adamson, T. C., JR., and Nicholls, J. A., "On the Structure of Jets from Highly Underexpanded Nozzle into Still Air," *Journal of the Aero/Space Sciences*, Jan. 1959, pp. 16–24.

[7] Ashkenas, H., and Sherman, F. S., "The Structure and Utilization of Supersonic Free Jets in Low Density Wind Tunnels," *Rarefied Gas Dynamics*, Vol. 2, 1966, pp. 84–105.

[8] Powell, A., "The Sound-Producing Oscillations of Round Underexpanded Jets Impinging on Normal Plates," *Journal of the Acoustical Society of America*, Vol. 83, No. 2, 1988, pp. 515–533.
doi:10.1121/1.396146

[9] Billig, F. S., Orth, R. C., and Lasky, M., "A Unified Analysis of Gaseous Jet Penetration," *AIAA Journal*, Vol. 9, No. 6, 1971, pp. 1048–1058.
doi:10.2514/3.49916

[10] Saito, T., Nakatsuji, H., and Teshima, K., "Numerical Simulation and Visualization of Freejet Flow-Fields," *Transactions of the Japan Society for Aeronautical and Space Sciences*, Vol. 28, No. 82, 1986, pp. 240–247.

[11] Narayanan, A. K., and Damodaran, K. A., "Mach Disk of Dual Coaxial Axisymmetric Jets," *AIAA Journal*, Vol. 31, No. 7, 1993, pp. 1343–1345.
doi:10.2514/3.49070

[12] Addy, A. L., "Effects of Axisymetric Sonic Nozzle Geometry on Mach Disk Characteristics," *AIAA Journal*, Vol. 19, No. 1, 1981, pp. 121–122.
doi:10.2514/3.7751

[13] Lengrand, J. C., Allegre, J., and Raffin, M., "Underexpanded Free Jets and Interaction with Adjacent Surfaces," *AIAA Journal*, Vol. 20, No. 1, 1982, pp. 27–28.
doi:10.2514/3.51040

[14] Cumber, P. S., Fairweather, M., Falle, S. A. E. G., and Giddings, J. R., "Predictions of the Structure of Turbulent, Highly Underexpanded Jets," *Journal of Fluids Engineering*, Vol. 117, No. 4, 1995, pp. 599–604.
doi:10.1115/1.2817309

[15] Matsuo, S., Tanaka, M., Otobe, Y., Kashimura, H., Kim, H.-D., and Setoguchi, T., "Effect of Axisymmetric Sonic Nozzle Geometry on Characteristics of Supersonic Air Jet," *Journal of Thermal Science*, Vol. 13, No. 2, 2004, pp. 121–126.
doi:10.1007/s11630-004-0019-2

[16] Otobe, Y., Kashimura, H., Matsuo, S., Setoguchi, T., and Kim, H.-D., "Influence of Nozzle Geometry on the Near-Field Structure of a Highly Underexpanded Sonic Jet," *Journal of Fluids and Structures*, Vol. 24, No. 2, 2008, pp. 281–293.
doi:10.1016/j.jfluidstructs.2007.07.003

[17] Lewis, C. H., Jr., and Carlson, D. J., "Normal Shock Location in Underexpanded Gas and Gas-Particle Jets," *AIAA Journal*, Vol. 2, No. 4, 1964, pp. 776–777.
doi:10.2514/3.2409

[18] Bauer, A. B., "Normal Shock Location in Underexpanded Gas-Particle Jets," *AIAA Journal*, Vol. 3, No. 5, 1965, pp. 1187–1189.

[19] Baek, S.-C., Kwon, S.-B., Kim, H.-D., Setoguchi, T., and Matsuo, S., "Study of Moderately Underexpanded Supersonic Moist Air Jets," *AIAA Journal*, Vol. 44, No. 7, 2006, pp. 1624–1627.
doi:10.2514/1.10029

[20] Otobe, Y., Matsuo, S., Tanaka, M., Kashimura, H., and Setoguchi, T., "A Study on Characteristics of Under-Expanded Condensing Jet," *JSME International Journal, Series B (Fluids and Thermal Engineering)*, Vol. 49, No. 4, 2006, pp. 1165–1172.
doi:10.1299/jsmeb.49.1165

[21] Irie, T., Yasunobu, T., Kashimura, H., and Setoguchi, T., "Hysteresis Phenomena of Mach Disk Formation in an Underexpanded Jet," *Theoretical and Applied Mechanics Japan*, Vol. 53, National Committee for Theoretical and Applied Mechanics, Tokyo, Japan, 2004, pp. 181–187.

[22] Sislian, J. P., "Condensation of Water Vapour with or without a Carrier Gas in a Shock Tube," Univ. of Toronto Inst. for Aerospace Studies, Toronto, Rept. 201, 1975, p.201.

[23] Adam, S., "Numerische und Experimentelle Untersuchung Instationarer Dusenstromungen mit Energiezufuhr durch Homogene Kondensation," Ph.D. Dissertation, Fukaltat fur Maschinenbau, Univ. Karlsruhe, Germany, 1999.

[24] Matsuo, S., Tanaka, M., Setoguchi, T., and Kaneko, K., "Effect of Non-Equilibrium Condensation of Moist Air on Flow Fields in a Ludwieg Tube (Case Without Condensation Upstream of Nozzle)," *Transactions of the Japan Society of Mechanical Engineers*, Vol. 69, No. 681, B, 2003, pp. 1163–1170 (in Japanese).

[25] Goldberg, U. C., "Exploring a Three-Equation R-k-ε Turbulence Model," *Journal of Fluids Engineering*, Vol. 118, No. 4, 1996, pp. 795–799.
doi:10.1115/1.2835511

[26] Heiler, M., "Instationäre Phänomene in Homogen/Heterogen Kondensierenden Düsen-und Turbinen-stormungen," Dissertation, Fakultät für Maschinenbau, Univ. Karlsruhe (TH), Germany, 1999.

[27] Goldberg, U. C., "Toward a Pointwise Turbulence Model for Wall-Bounded and Free Shear Flows," *Journal of Fluids Engineering*, Vol. 116, No. 1, 1994, pp. 72–76.
doi:10.1115/1.2910245

[28] Yamamoto, S., and Daiguji, H., "Unsteady Navier–Stokes Simulation of Turbulent Flows through a Supersonic Compressor Cascade," *Proceedings of the ASME Fluids Engineering Division*, Vol. 120, American Society of Mechanical Engineers, Fairfield, NJ, 1991, pp. 73–79.

[29] Yee, H. C., "A Class of High-Resolution Explicit and Implicit Shock Capturing Methods," NASA TM-101088, 1989.

[30] Nebbache, A., and Pilinski, C., "Pulsatory Phenomenon in a Thrust Optimized Contour Nozzle," *Aerospace Science and Technology*, Vol. 10, No. 4, 2006, pp. 295–308.
doi:10.1016/j.ast.2005.07.002

J. Sahu
Associate Editor